Inorganic Chemistry

Article

pubs.acs.org/IC

Preparations, Crystal Structures, and Magnetic Properties of *N,N*-Dipyridylaminoxyl as a New Magnetic Coupler and Its One-Dimensional Cobalt(II) Chains

Kensuke Murashima,[†] Takeaki Watanabe,[†] Shinji Kanegawa,[†] Daisuke Yoshihara,[†] Yuji Inagaki,[‡] Satoru Karasawa,[†] and Noboru Koga*[,†]

[†]Graduate School of Pharmaceutical Sciences, Kyushu University, 3-1-1 Maidashi, Higashi-ku, Fukuoka, 812-8582 Japan

[‡]Department of Applied Quantum Physics, Kyushu University, 744 Motooka, Nishi-ku, Fukuoka, 812-0395 Japan

Supporting Information

ABSTRACT: *N,N*-Dipyridilaminoxyl, **NOpy$_2$**, having a stable aminoxyl, was prepared as a new magnetic coupler for heterospin systems. Solutions of **NOpy$_2$** were mixed with those of bis{1,1,1,5,5,5, hexafluoro-4-(phenylimino)-2-pentanonate}cobalt derivatives, Co(hfpip-X)$_2$, at a 1:1 ratio to afford the polymeric cobalt(II) complexes, [Co(hfpip-X)$_2$(**NOpy$_2$**)]$_n$; X = H (**1**), F (**2**), F$_3$ (**3**), F$_5$ (**4**), Cl (**5**), Cl$_3$ (**6**), Br (**7**), and I (**8**) as single crystals. In all complexes, the local structures of the cobalt-complex units were compressed octahedra and the pyridine ligands in **NOpy$_2$** units coordinated to the cobalt ions in trans configuration to form linear chains for **1**−**4** and in cis configuration to form helical chains for **5**−**8**. In the chains, the aminoxyl in **NOpy$_2$** ferromagnetically interacted with the cobalt ions to produce the ferromagnetic chains with J_{intra}/k_B = 9−14 K. In the magnetic susceptibility experiments of aligned sample of **6**, the magnetic easy axis was determined to be the *a** axis, which was the direction perpendicular to the *b* axis of the chain axis. The resulting chains, all except **4**, interacted antiferromagnetically among each other, and especially in **1**, **5**, **7**, and **8**, the magnetic behaviors characteristic to canted two-dimensional (2D) antiferromagnets with T_c = 5.6, 4.0, 4.0, and 6.2 K, respectively, were observed. All complexes showed slow magnetic relaxations affected by the interchain antiferromagnetic interaction. The effective activation barriers, Δ_{eff}/k_B, for the reorientation of the magnetism for all complexes except **4** were estimated to be 25−39 K in the presence of a direct current (dc) field.

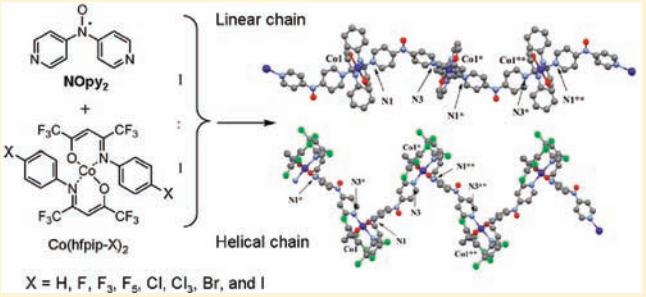

INTRODUCTION

Among the molecule-based magnets,[1] the single-molecule magnet (SMM)[2] and single-chain magnet (SCM)[3] having uniaxial anisotropies have attracted much attention. They have a characteristic magnetism showing magnetic hysteresis accompanied by slow magnetic relaxation because of the anisotropic barrier. In SMM and SCM behaviors, furthermore, a spin quantum tunneling effect is observed at extremely low temperature.[2,3g,h] Because SMMs and SCMs show this unique magnetism different from that of classical bulk magnets and because they are of nanometer size, they have been intensively studied in the fields of material science and fundamental magnetic chemistry.[2,3] Well-defined molecules are Mn12[2a] and their analogues[2a−h] for SMMs and [Co(hfac)$_2$(NITPhOMe)]$_n$[3a] and the family of [Mn$_2$(saltmen)$_2$Ni(pao)$_2$(L)$_n$](anion)$_2$ complexes[3b] for SCMs. For the construction of new molecule-based magnets, we previously proposed the use of a heterospin system[4] consisting of the 3d spins of the metal ion and the 2p spins of the unpaired electrons of the organic spins coupled magnetically through aromatic ligands. In the heterospin systems, high-spin carbenes and aminoxyls, which are reactive intermediates and stable radicals, respectively, have been used as organic spin sources. The most impressive characteristic of this heterospin system is the possibility of constructing the unique molecule-based magnets by systematically varying the combinations of the organic spins and the metal ions. In constructing such SMMs,[5,8,9] the combination of an anisotropic metal ion, cobalt(II) ion, and monopyridyl ligands having an organic spin were employed. The obtained discrete heterospin Co(II) complexes showed SMM behaviors with relatively large effective activation barriers, U_{eff}/k_B (= 29−139 K), for the reorientation of magnetism and large coercive forces, H_c, in hysteresis loops at temperatures higher than 2 K.[6,7] These studies indicated the usefulness of the heterospin system for the construction of SMMs.[5] When the construction of a one-dimensional (1D) chain was considered as an extension of the heterospin studies, a magnetic coupler bridging two metal complexes through an organic spin was required. In the system using carbene as the organic spin source, the monodiazo-dipyridyl ligand, **D1py$_2$**, which was a precursor of dipyr-

Received: November 8, 2011
Published: April 10, 2012

   dx.doi.org/10.1021/ic202397m | *Inorg. Chem.* 2012, 51, 4982−4993

idylcarbene, **C1py$_2$**, had been already prepared as a photoresponsive magnetic coupler.[4] The 1:1 polymeric complexes, [Mn- and Cu(hfac)$_2$**D1py$_2$**]$_n$; hfac = hexafluoroacetylacetonato, in combination with **D1py$_2$** and the relatively small anisotropic metal complexes, Mn- and Cu(hfac)$_2$ have been reported to form ferri- and ferromagnetic chains, respectively, after irradiation.[6,7] Recently, we applied the heterospin system using **D1py$_2$** to the anisotropic metal complex and found that the cobalt complex chains after irradiation of [Co(hfpip)$_2$**D1py$_2$**]$_n$; hfpip = 1,1,1,5,5,5-hexafluoro-4-(phenylimino)-2-pentanonate, showed slow magnetic relaxation behaviors with Δ_{eff}/k_B values of about 90 K.[8] In the stable aminoxyl spin system on the other hand, *N*,*N*-dipyridylaminoxyl, **NOpy$_2$**, corresponding to **C1py$_2$**, would be a promising candidate for a new magnetic coupler. This time, **NOpy$_2$** was successfully prepared, and the 1:1 polymeric complexes of Co(hfpip)$_2$ with **NOpy$_2$** were obtained. We report here the preparation, the molecular structure, and the magnetic properties of a new magnetic coupler, **NOpy$_2$**, and the 1:1 polymeric complexes of Co(hfpip-X)$_2$; X = H, F, F$_3$, F$_5$, Cl, Cl$_3$, Br, and I, with **NOpy$_2$**. In this study, the magnetic property of the 1:2 complex, [Co(hfpip)$_2$(**4NOpy**)$_2$], which showed SMM behavior with U_{eff}/k_B = 29 K in a frozen solution,[9] was considered to be the reference.

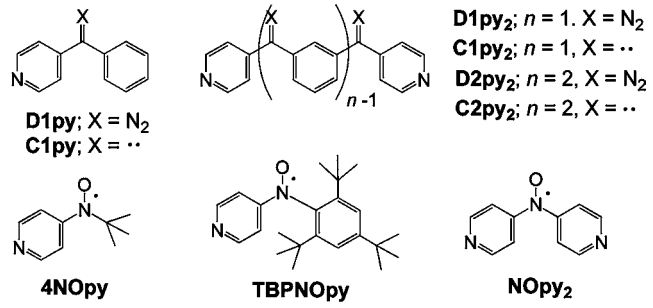

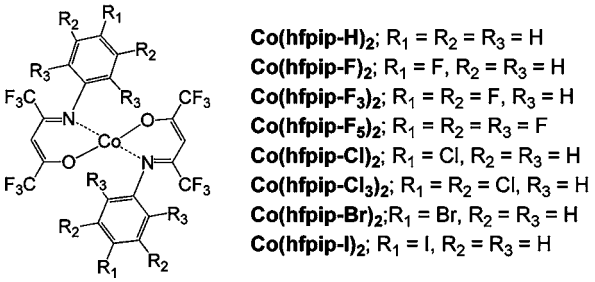

RESULTS AND DISCUSSION

Preparations of NOpy$_2$ and Polymeric Complexes of Co(hfpip-X) with NOpy$_2$. The magnetic coupler, **NOpy$_2$**, bridging the metal ions was successfully prepared in relatively high yield, according to the preparation route shown in Scheme 1. A key compound 4-nitrosopyridine, **NOpy**, was prepared by the reduction of 4-nitropyridine with zinc powder and then by oxidation with $Na_2Cr_2O_7$. The metalation of 4-iodopyridine with ethylmagnesium bromide, followed by a reaction with **NOpy**, afforded the hydroxyamine derivative, **NOHpy$_2$**, as a pale yellow powder. The oxidation of **NOHpy$_2$** with freshly prepared Ag_2O gave **NOpy$_2$**. The single crystal was obtained as red block crystals by slow evaporation of the solution of **NOpy$_2$** in a mixture of CH_2Cl_2 and *n*-hexane. Although **4NOpy** was

Scheme 1. Preparation of NOpy$_2$

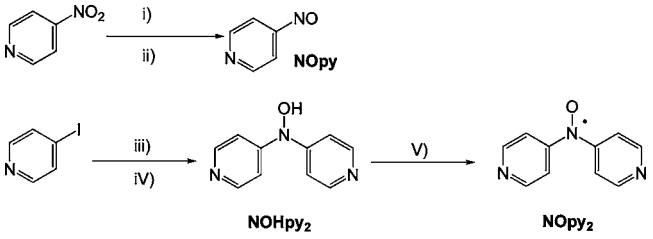

i) Zn, NH_4Cl, MeOH ii) $Na_2Cr_2O_7 \cdot 2H_2O$, aq. H_2SO_4, iii) EtMgBr, THF iv) **NOpy**, THF v) Ag_2O, CH_2Cl_2

easily polymerized in isolation as a solid, the **NOpy$_2$** obtained was relatively stable in the solid state and in solutions of organic solvents and even water.

The solution of **NOpy$_2$** in CH_2Cl_2 was red, and its UV−vis spectrum (Figure 1) showed absorptions at 271 (ε = 10500),

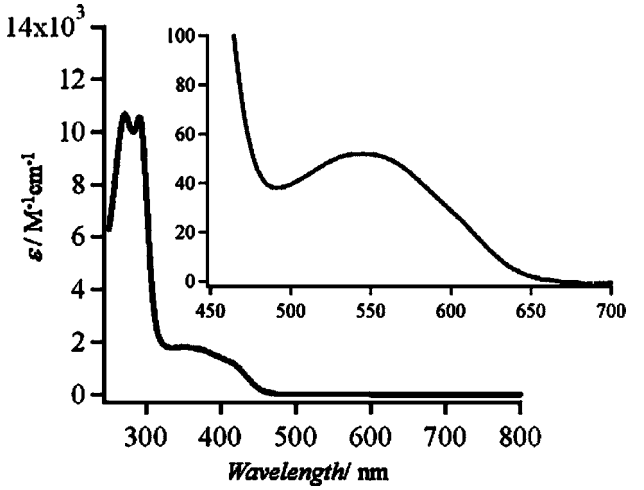

Figure 1. UV−vis spectrum of **NOpy$_2$** in CH_2Cl_2. The inset shows the expanded visible region.

290 (10300), and 360 nm (shoulder, 1600) in addition to 546 (ε = 42) nm due to the *n*-π* transition. The absorption at 546 nm was a longer wavelength by 27 nm compared with that (λ_{max} = 519 nm) for **4NOpy**.[10]

The bidentate chelating cobalt complexes, Co(hfpip-X)$_2$, which attach various electron donating and withdrawing substituents (X) to the phenyl ring, were used for this heterospin system, and the complexation with **NOpy$_2$** was carried out. The substituted Co(hfpip)$_2$ was prepared in a manner similar to the modified procedure for the unsubstituted one.[5e,9,11] The solution of **NOpy$_2$** was mixed with that of Co(hfpip-X)$_2$ in a 1:1 molar ratio and then left at −3 or 4 °C for 2 days. Only the complexes of **NOpy$_2$**−Co(hfpip-X)$_2$, X = H, F, F$_3$, F$_5$, Cl, Cl$_3$ Br, and I, having the halogen substituents and no substituent, were obtained as single crystals. The polymeric 1:1 complexes were obtained as dark red crystals with formulas [Co(hfpip-X)$_2$(**NOpy$_2$**)]$_n$; X = H (**1**), F (**2**), F$_3$ (**3**), F$_5$ (**4**), Cl (**5**), Cl$_3$ (**6**), Br (**7**), and I (**8**). All of the complexes obtained were stable under ambient atmosphere.

Crystal Structure Analysis. The single crystals of **NOpy$_2$** and complexes, **1**−**8**, were analyzed by X-ray crystallography (Supporting Information, Table S1).

*(A). **NOpy$_2$**.* An ORTEP drawing of the molecular structure is shown in Figure 2a. **NOpy$_2$** has no symmetry operation

dx.doi.org/10.1021/ic202397m | *Inorg. Chem.* 2012, 51, 4982−4993

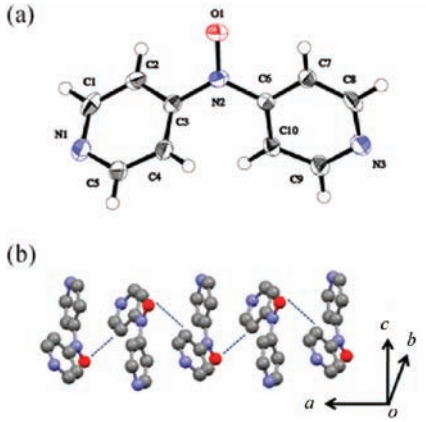

Figure 2. (a) ORTEP drawing of molecular structure of **NOpy$_2$** and (b) its crystal packing with ball and stick model (C; gray, O; red, and N; blue). Hydrogen atoms are omitted for clarity. The broken lines indicate the short distance ($O_{aminoxyl}$-$C2_{py}$) of 3.52 Å.

within the molecule. The length of NO bond is 1.29 Å, and the dihedral angles between the aminoxyl plane and the pyridine plane, NO-py; C3N2O1−N1C2C4 and C3N2O1−N3C7C10, and py-py between the pyridine rings, were 18.8 and 41.4°, and 55.9°, respectively. The observed dihedral angle, NO-py, was relatively small, indicating that the aminoxyl spins effectively delocalize on both sides of the pyridine ring. In the crystal packing (Figure 2b), the molecules were aligned head-to-tail alternately along the *a* axis. The intermolecular distance between aminoxyl centers was 5.23 Å, which was too far to directly and magnetically interact. The nearest distance was 3.52 Å of O−C2′ between the oxygen for the aminoxyl center and the C2′ carbon of pyridine ring belonging to the neighbor molecule. The observed short distance might suggest that magnetic couplings between the molecules take place to form a chain magnetically.

*(B). [Co(hfpip-X)$_2$(**NOpy$_2$**)]$_n$; X = H (**1**), F (**2**), F$_3$ (**3**), F$_5$ (**4**), Cl (**5**), Cl$_3$ (**6**), Br (**7**), and I (**8**).* X-ray crystallography of the single crystals revealed that all complexes had chain structures in trans coordination for **1**−**4** and in cis coordination for **5**−**8**. The crystals of **5**−**8** contained the solvent molecules and those for **1**−**4** did not. The solvent molecules were located between the chains. Disorders of pentafluorophenyl rings in **4** were observed. The chains of **2**, **3**, and **4** had an intrachain symmetry center at the cobalt ion, in which **2** contained two crystallographically different cobalt ions (Co1 and Co2), while those of **1** and **5**−**8** had a symmetry center between the chains. Furthermore, chains **1**, **2**, and **5**−**8** had **NOpy$_2$** units having two kinds of pyridine (A and B), which were connected alternately in the order ---A-B, Co, A-B, Co, A-B --- for **1** and **5**−**8** and in the order --- A-B, Co1, B-A, Co2, A-B --- for **2**. Chains **3** and **4** had a single pyridine A and the connecting mode of --- A-A, Co, A-A ---. The schematic drawings of the connecting mode for **1**−**4** and **5**−**8** are shown in Supporting Information, Figure S1. The local cobalt complex units in the cobalt(II) chains had similar six coordination structures, in which each cobalt ion is surrounded by two nitrogen atoms (N_{Py}) of pyridine rings, two (N_{im}) of imine in hfpip at the basal plane, and two oxygen atoms of hfpip at the apical positions. ORTEP drawings of the partial structures of the cobalt complex units are shown in Figure 3 for **1**, **2**, and **6**, and in Supporting Information, Figure S2, for the others.

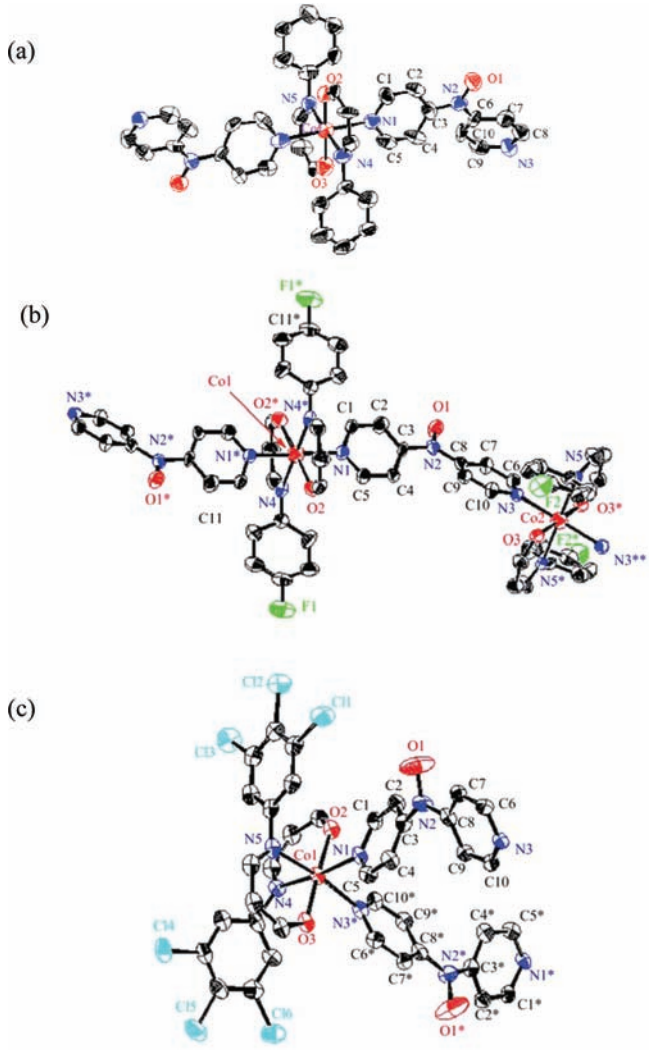

Figure 3. ORTEP drawings of the partial structure of the cobalt complex units in (a) **1**, (b) **2**, and (c) **6**. Hydrogen atoms, CF_3 groups, and solvents are omitted for sake of clarity.

The molecular structures of the cobalt complex units in all complexes were compressed octahedrons, in which the bond lengths of r_{Co-O} between the cobalt ion and the oxygen of hfpip as the axial ligand were shorter by 0.15−0.20 Å compared with those (r_{Co-Npy} and r_{Co-Nim}) between the cobalt ion and the nitrogen of pyridine and hfpip. The bond lengths of r_{Co-O} were 2.01−2.03 Å for **1**−**3** and 2.02−2.03 Å for **5**−**8**. In contrast, the bond length of Co−N_{py} (r_{Co-Npy} = 2.24 Å) for **4** was longer than that of Co−N_{im} (r_{Co-Nim} = 2.15 Å) with corresponding lengths (r_{Co-Npy} = 2.18−2.19 Å for **1**−**3** and 2.16−2,21 Å for **5**−**8**) in the other complexes, suggesting that the magnetic exchange coupling parameter, J_{intra}, between the aminoxyl and the cobalt ion might be weak. The observed long bond length might be caused by the van der Waals contact between the F atom at the C2 position of the phenyl ring in Co(hfpip-F_5)$_2$ and the C2 atom of the pyridine ring.

In the dihedral angles (py-XY) between the pyridine ring and the XY plane defined by the four nitrogen atoms, which might affect J_{intra} and *E*, the zero-field splitting parameter, py-XY of 55.6° for **3** was smaller than those for others in the range of 72.4−83.4° for **1**, **2**, and **4** and 65.4−70.2° for **5**−**8**. Therefore, the magnetic coupling for **3** might be weak compared with the

dx.doi.org/10.1021/ic202397m | *Inorg. Chem.* 2012, 51, 4982−4993

others.[8] The dihedral angles, py-NO, between the pyridine ring and the aminoxyl plane were 16.0−31.8° for **1**−**4** and 16.0−31.2°for **5**−**8**, which were comparable with the values (18.8 and 41.8°) for **NOpy$_2$** in metal free, suggesting that the magnetic coupling between the aminoxyl and the cobalt ion took place effectively. The distances of O_{NO}−O_{NO} and Co−Co within the chain were in the range of 14.0−14.4 and 11.1−11.7 Å, respectively, for **1**−**4** and 10.5−10.8 and 11.3−11.8 Å, respectively for **5**−**8**, indicating that the direct interactions of spin centers were insignificant.

In the complexes, the pyridines of **NOpy$_2$** coordinated to the cobalt ions in trans configuration for **1**−**4** to form linear chains and in cis conformation for **5**−**8** to form helical chains. In the trans chains for **1**, **2**, **3**, and **4**, the cobalt complex units aligned to one position along the $a - c$, $b + c - a$, $a + c$, and c axis, respectively, which were the chain direction, while in the cis chains, **5**−**8**, they were located in two positions along the b axis. In all complexes, the directions of the z axis of the O−Co−O bond, which was short in a compressed octahedron of Co(hfpip)$_2$ units, were different from those of the chain, and the angles between the two axes were large. In the trans complexes, the z axes had angles of 64, 63 and 65, 69, and 61° for **1**, **2**, **3**, and **4**, respectively, toward the chain axis, while in cis complexes the angles were 63, 68, 63, and 65° for **5**, **6**, 7, and **8**, respectively, toward the b axis of the chain axis. The observed large angles between the z and the chain axes were anticipated to affect the magnetic properties of the heterospin chains. The angles between the z and the chain axes are summarized in Supporting Information, Table S2.

The crystal packings as a wire frame model are shown in Figure 4 for **1** and **5** and in Supporting Information, Figure S3, for the others.

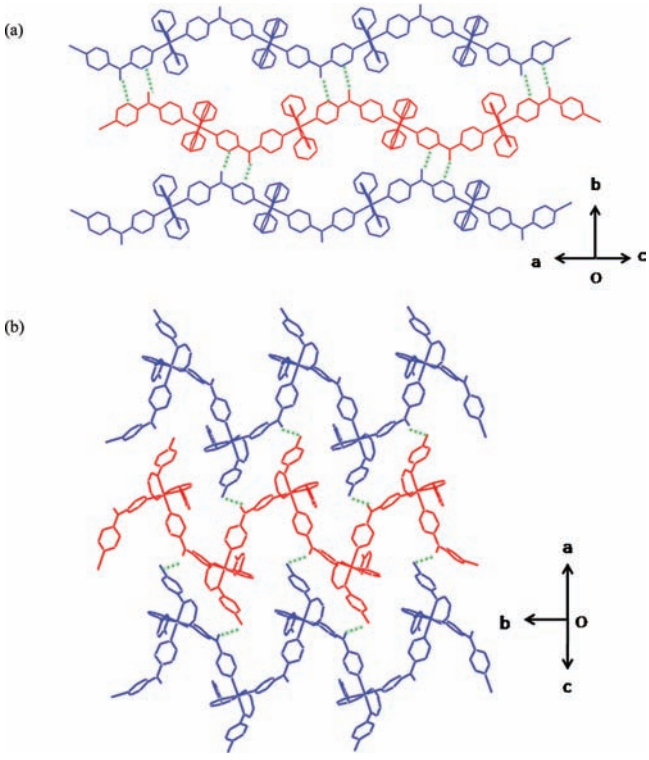

Figure 4. Crystal packings as wire and frame models of **1** (a) and **5** (b). Hydrogen atoms, CF_3 groups, and solvents are omitted for sake of clarity. Short contacts are indicated by the dotted lines.

As shown in Figure 4, the chains (blue and red chains) for all complexes alternately align in parallel to form a two-dimensional (2D) sheet structure. Chains **1** and **2** had the short NO---C_β distance of $r_{NO\text{-}C\beta}$ = 3.25 (Figure 4a) and 3.26 Å, respectively, between the aminoxyl and the C_β carbon in pyridine and formed 2D sheet structures. These short contacts were also observed in the crystal of **NOpy$_2$**. Considering the relative geometry of the π orbitals between the aminoxyl and the pyridine ring (Supporting Information, Figure S4), the π−π overlaps in **1** and **2**, in which the π orbitals are parallel to each other, were ineffective, while that of **NOpy$_2$** was favorable. Although the $r_{NO\text{-}C\beta}$ distances of **1** and **2** are shorter than that for **NOpy$_2$**, the through-space NO---C_β magnetic interactions in **1** and **2** might therefore be weaker than that of **NOpy$_2$**. In chain **2**, additional short interplane distances of r_{NO-CF} = 3.42 Å were observed between the aminoxyl center and the carbon (C_F) attached fluoride. Although the other complexes had no NO---C_β short contact between the chains, they, except for **4** and **6**, had short distances between NO and halogen (X) ($r_{NO\text{-}X}$; X = F, Cl, Br, and I) of 3.29, 3.62, 3.64, and 3.68 Å for **3**, **5** (Figure 4b), 7, and **8**, respectively, to form a 2D sheet structure. The distance of $r_{NO\text{-}X}$ increased in the order **3** < **5** < **7** < **8**. Taking the radius of the halogen atom into account,[12] the van der Waals distance of $r_{NO\text{-}X}$ became longer in the order **8** < **7** < **5** < **3**. However, the magnetic interaction through NO---X might be anticipated to be weak. Chain **4** had no short contacts within 4 Å between the chains except for the disordered position of pentafluorophenyl rings, $r_{NO\text{-}F}$ = 3.43 Å. In chain **6**, no significant short distances within 4 Å were observed. The only short distances observed between the chains were $r_{NO\text{-}F}$ = 2.73 and 3.03 Å of NO---F between the aminoxyl center and the CF_3 group. The magnetic interaction through them might be presumably weaker. The selected bond lengths, dihedral angles, angles between the z and the chain axes, and the nearest distances between the chains for **1**−**4** and **5**−**8** are summarized in Supporting Information, Table S2.

Magnetic Properties. The magnetic properties of **NOpy$_2$** in solution and crystalline state were investigated by electron spin resonance (ESR) spectrometry and superconducting quantum interference device (SQUID) magneto/susceptometry, respectively. Those for polymeric cobalt complexes, **1**−**8**, in the crystalline state were also investigated by SQUID magneto/susceptometry.

*(A). **NOpy$_2$**. (A-1). In Solution.* The ESR spectrum (9.4 GHz) at 25 °C for the solution sample (~1 mM) of **NOpy$_2$** in degassed toluene is shown in Figure 5 together with the simulation spectrum.

The spectrum showed a three-line signal (signal intensity; 1:1:1), in which each signal was split into many lines because of the nuclear spins of the nitrogen and hydrogen. The spectrum was simulated with WinSIM ver. 0.96 software[13] to give g = 2.0071 and hyperfine coupling constants (hfc), a_N = 8.52 (N_{NO}) and 0.94 (N_{py}) gauss for the nitrogens of the aminoxyl center and pyridine, respectively, and a_H = 1.69 (C3) and 0.60 (C2) gauss for the hydrogens at the 3- and 2-positions of pyridine, respectively. The corresponding values for **4NOpy** in CH_2Cl_2 are a_N = 11.0 (N_{NO}) and 2.1 (N_{py}) gauss and a_H = 1.35 (C3) and 0.61 (C2) gauss.[10] The decrease in the hfc value due to the nitrogen of pyridine for **NOpy2** indicated the decrease of the spin density on the nitrogen. Therefore, the magnetic coupling between the aminoxyl and the metal ion in **NOpy$_2$** complex might be weaker than that in the **4NOpy** complex.

dx.doi.org/10.1021/ic202397m | *Inorg. Chem.* 2012, 51, 4982−4993

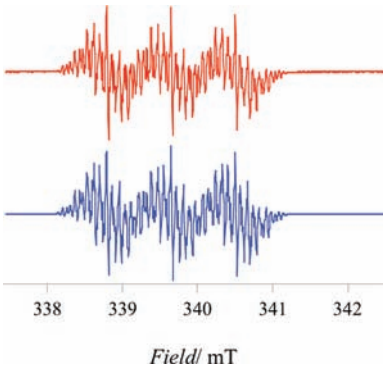

Figure 5. ESR spectrum (9.4 GHz) of **NOpy$_2$** in toluene at 25 °C; (red) experimental and (blue) simulation.

(A-2). In Solid State. ESR spectrum of a powder sample of **NOpy$_2$** showed one broad signal at $g \approx 2.008$ (Supporting Information, Figure S5). The direct current (dc) magnetic susceptibility (χ_{mol}) for a pulverized sample of **NOpy$_2$** was measured at a constant field of 5 kOe in the temperature range of 2−300 K. Temperature dependence of the χ_{mol} is shown as a $\chi_{mol}T$ vs T plot together with χ_{mol} vs T plot in Figure 6. In the

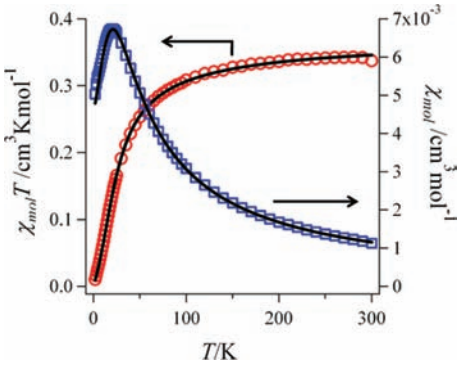

Figure 6. $\chi_{mol}T$ vs T and χ_{mol} vs T plots for **NOpy$_2$**. The solid line shows a best-fit result by the antiferromagnetic 1D model (see text).

χ_{mol} vs T plot, on cooling, the χ_{mol} values gradually increased, reached the maximum (6.7×10^3 cm^3 mol^{-1}) at 20 K, and then decreased below it. In the $\chi_{mol}T$ vs T plot, the $\chi_{mol}T$ value at 290 K is 0.342 cm^3 K mol^{-1} and is consistent with that (0.375) calculated using a spin-only equation with $S = 1/2$. On cooling from 290 K, the $\chi_{mol}T$ values gradually decreased and reached zero at 2 K. The observed thermal profiles of χ_{mol} and $\chi_{mol}T$ values indicated that a strong antiferromagnetic interaction was in effect.

To understand the magnetic properties quantitatively, an antiferromagnetic chain model,[14] $H = -J\sum_i S_i \cdot S_{i+1}$, suggested by X-ray crystal structure analysis was applied to the spin system. The experimental data fit the theoretical equation, in which a mass factor, w, and $g = 2.0069$ obtained from the ESR spectra of powdered samples were used. The best-fitting parameters were the spin exchange coupling parameters $J/k_B = -32.4$ K and $w = 0.98$, and the best-fitting result is shown in Figure 6 as a solid curve.

*(B). [Co(hfpip)$_2$(**NOpy$_2$**)$_n$] Complexes.* The static and dynamic magnetic properties of **1**−**8** were investigated by dc and alternating current (ac) magnetic susceptibility measurements, respectively.

*(B-1). Static Magnetic Properties of **1**−**8**. (i). Plots of χ_{mol}^{-1} vs T and $\chi_{mol}T$ vs T for **1**−**8**.* The dc molar magnetic susceptibilities (χ_{mol}) for the pulverized samples of **1**−**8** were measured at a constant field of 5 and 1 kOe in the temperature ranges of 2−300 K and below 30 K, respectively. Temperature dependences of the χ_{mol} for all complexes are shown as the $\chi_{mol}T$ vs T plots in Figure 7 and as the χ_{mol}^{-1} vs T and χ_{mol} vs T plots in Supporting Information, Figures S6 and S7, respectively.

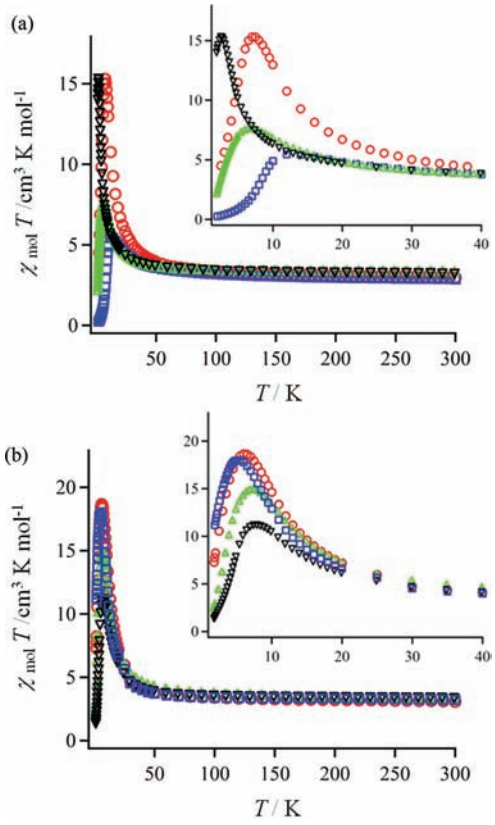

Figure 7. Plots of $\chi_{mol}T$ vs T for (a) trans chains; **1** (red circle), **2** (blue square), **3** (green triangle), and **4** (black reverse triangle) and (b) cis chains; **5** (red circle), **6** (blue square), **7** (green triangle), and **8** (black reverse triangle) at a constant field of 5 and 1 kOe in the temperature ranges of 2−300 K and below 30 K, respectively. Insets show the expanded low temperature region (1.9−40 K).

In the $\chi_{mol}T$ vs T plots, the $\chi_{mol}T$ values were nearly constant in the temperature range of 300−100 K and those at 300 K were 2.96, 2.87, 3.28, 3.15, 3.07, 3.21, 3.19, and 3.27 cm^3 K mol^{-1} for **1**, **2**, **3**, **4**, **5**, **6**, **7**, and **8**, respectively. These values were consistent with those (2.5−2.9) calculated by a spin-only equation with isolated cobalt ion ($S = 3/2$ and $g = 2.25$−2.46) and aminoxyl ($S = 1/2$ and $g = 2.00$). The g values for Co ion, g_{Co}, calculated from the $\chi_{mol}T$ values at 300 K were in the range of 2.25−2.46, which were consistent with the g_{Co} values for [Co(hfpip)$_2$(**4NOpy**)$_2$] derivatives reported previously.[9] On cooling, the $\chi_{mol}T$ values gradually increased below 100 K, steeply increased below 40 K, reached a maximum, and then steeply decreased. In the complexes, **1**−**4**, the $\chi_{mol}T$ values showed different thermal profiles in the temperature region below 40 K. **1**−**4** had maximum $\chi_{mol}T$ values of 15.3, 5.46, 7.57, and 15.2 cm^3 K mol^{-1} at 7.5, 12.0, 7.0, and 2.6 K, respectively, while **5**−**8** showed similar thermal profiles of the $\chi_{mol}T$ value

dx.doi.org/10.1021/ic202397m | Inorg. Chem. 2012, 51, 4982−4993

Table 1. Values of J/k_B and Δ/k_B in Branch Chain Model,[15] Curie–Weiss Parameters (C and θ), and g_{Co}

	1	2	3	4	5	6	7	8
J_{intra}/k_B (K)	14.4	10.6	8.5	8.8	12.8	11.5	14.0	11.5
Δ/k_B (K)	283	289	370	296	315	405	280	361
C (cm^3 K mol^{-1})	2.84	2.79	3.26	3.09	3.00	3.17	3.10	3.21
θ (K)	14.6	11.7	5.23	7.70	11.7	7.90	14.9	7.99
g_{Co}	2.30	2.25	2.48	2.33	2.37	2.46	2.41	2.46

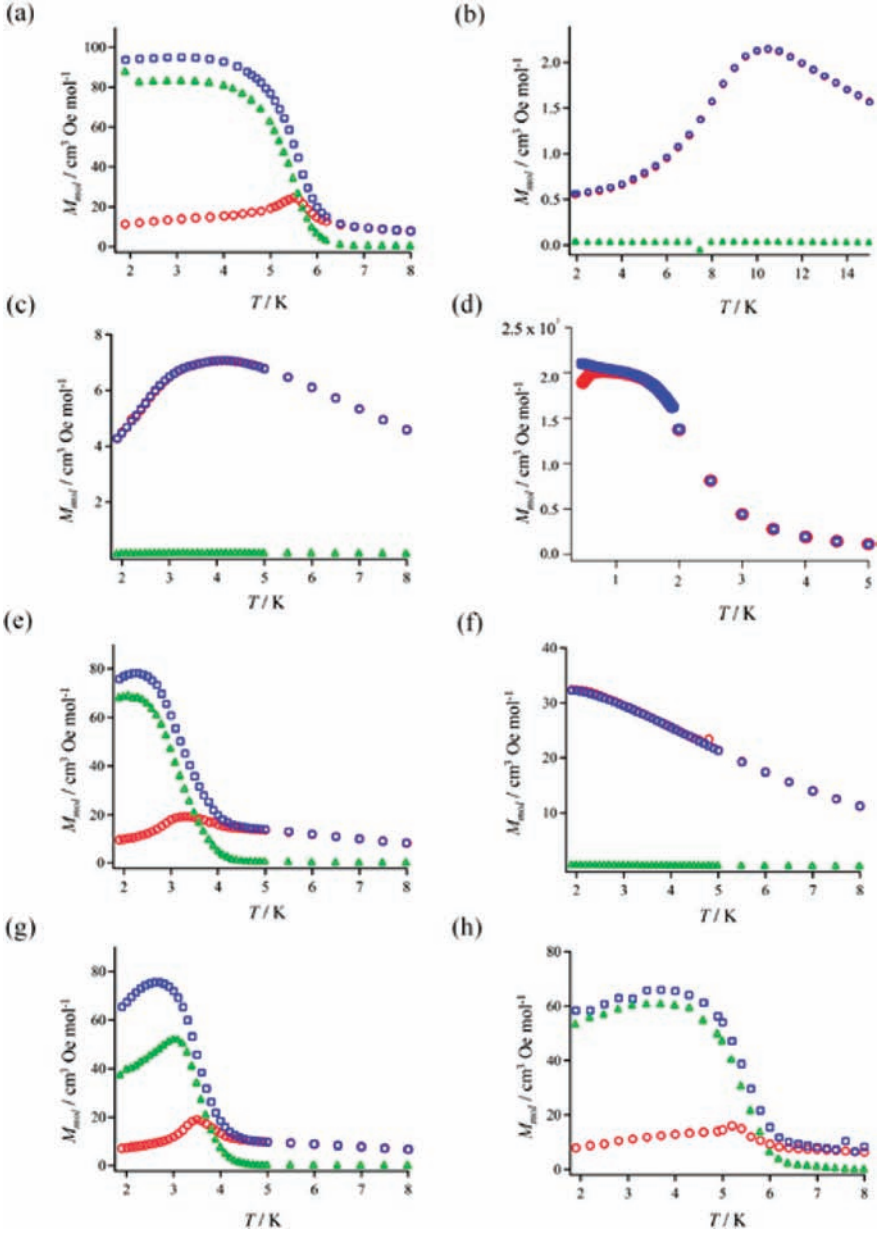

Figure 8. M_{mol} vs T plot in a sequence of ZFCM (red circle), FCM (blue square), and RM (green triangle) with 4.7 Oe for the pulverized sample of **1** (a), **2** (b), **3** (c), **4** (d), **5** (e), **6** (f), 7 (g), and **8** (h).

but with maximum $\chi_{mol}T$ values of 18.7, 18.0, 14.9, and 11.1 cm^3 K mol^{-1} at 6.0, 5.5, 7.5, and 8.0 K, respectively. All maximum $\chi_{mol}T$ values were larger than the theoretical ones (2.4 cm^3 K mol^{-1}) calculated by the spin-only equation with isolated cobalt ion ($\chi_{mol}T$ of 2.0 cm^3 K mol^{-1} for Co(hfpip)$_2$ with an effective spin quantum number, S_{eff} = 1/2 and g = 4)[5f,9] and aminoxyl (S = 1/2 and g = 2.00). This observed increase in the $\chi_{mol}T$ values below 40 K indicated that ferromagnetic interactions within the chain operated, and the correlation length became longer with decreasing temperature until a certain point. The thermal profiles for fluoride complexes **2**–**4**, in which the $\chi_{mol}T$ values steeply increased at lower temperatures compared with those for the others (the inset of Figure 7a and b), suggested that the intrachain ferromagnetic interactions for **2**–**4** were weaker than those for **1** and **5**–**8**. From the increasing in $\chi_{mol}T$ value behavior below 40 K, the

dx.doi.org/10.1021/ic202397m | Inorg. Chem. 2012, 51, 4982–4993

magnitude of the intramolecular exchange parameters, J_{intra}, would be in order of **1**, **5** ~ **7** > **8** > **2**−**4**. The decrease in $\chi_{mol}T$ values in the extremely low temperature region might be due to interchain antiferromagnetic interaction in addition to an effect of the zero field splitting parameter caused by the spin−orbit coupling in the cobalt ion. Especially, the $\chi_{mol}T$ value at 1.9 K for **2** was nearly zero, indicating a strong antiferromagnetic interaction. In **1**−**8**, accordingly, the intra- and interchain magnetic interactions were ferromagnetic and antiferromagnetic, respectively. In trans complexes, **1**−**4**, the magnetic profile for **1** was different and closer to those for cis complexes, **5**−**8**, rather than those for **2**−**4**. From the temperature showing the maximum $\chi_{mol}T$ values in the $\chi_{mol}T$ vs T plots, the antiferromagnetic interactions were weaker in the order **2** > **3** > **4** for trans complexes and in the order **8** > **7** > **5** > **6** for cis complexes. To estimate the intramolecular exchange parameters, J_{intra}, for **1**−**8** quantitatively, a single J_{intra} parameter was assumed for the chains, and a branched chain model[15] (Supporting Information, Equation S1 in section S8 and Figure S7) was applied to this spin system, in which the octahedral high-spin Co(II) ions are orbitally degenerate ($^4T_{1g}$).[1,16] To reduce the number of parameters, six parameters in the branched model, the g_{Co} values calculated from the constant $\chi_{mol}T$ values in the high temperature region and g_{NO} = 2.0 were used and the J'/k_B and k values were fixed according to the literature (J'/k_B = −100 K and k = 0.8).[5f,9] The theoretical equation fitted the experimental data above 30 K by a least-squares method. The best fitting results for J_{intra}/k_B and Δ/k_B are listed in Table 1 together with the Curie−Weiss parameters and the g_{Co} values, which were obtained by the Curie−Weiss fit of the χ_{mol}^{-1} vs T plots (Supporting Information, Figure S6). The theoretical curves by a branched model are shown in the χ_{mol} vs T plots (Supporting Information, Figure S7) as solid lines.

The obtained J_{intra}/k_B and Δ/k_B values for all complexes were in the range of 8.5−14.4 and 280−400 K, respectively. The Δ/k_B values were reasonable as those for the octahedral cobalt complex.[16] The fitting results suggested that in all complexes the intrachain ferromagnetic interactions took place in the J_{intra}/k_B range of 8.5−14.4 K. The J_{intra}/k_B values for **3** and **4** were slightly smaller than those for the others. In **3** and **4**, the small dihedral angle of XY-py for **3** and long bond length of $r_{Co\text{-}py}$ = 2.24 Å for **4** might affect and weaken the intrachain ferromagnetic interaction. The θ values for all complexes obtained by the Curie−Weiss equation, which were positive, also indicated the ferromagnetic interaction. Additionally, in the χ_{mol} vs T plots for **1**, **2**, **3**, **5**, **7**, and **8**, an abrupt increase and decrease in the χ_{mol} value (cusp) with low dc field were observed at 5.8, 10.0, 4.1, 3.6, 4.6, and 5.5 K, respectively. The observed magnetic behaviors suggested a phase transition from the paramagnet phase (P) to the antiferromagnet phase (AF) in the low temperature region (see Figure 10 and Supporting Information, Figure S10′).

(ii). ZFCM, FCM, and RM Measurements. To understand the magnetic properties for the complexes in the low temperature region, the dc magnetic measurements were carried out using a sequence of the zero field-cooled magnetization (ZFCM), the field-cooled magnetization (FCM), and the remnant magnetization (RM) in the temperature range of 1.9−8.0 K for **1**, **3**, and **5**−**8** and 1.9−15 K for **2** and **4**. For ZFCM and FCM measurements, the constant dc field of 4.7 Oe was used. The M_{mol} vs T plot in a sequence of ZFCM, FCM, and RM for the pulverized sample of **1**−**8** are shown in Figure 8.

As shown in ZFCM, FCM, and RM measurements for **1** (Figure 8a), in ZFCM, the M_{mol} value being 11.3 $cm^3Oe\ mol^{-1}$ at 2 K, slightly increased until 4.6 K on warming, and then decreased, while in FCM, on cooling, the M_{mol} value steeply increased below 6.0 K. In RM, the M_{mol} value, being 88 cm^3 Oe mol^{-1} at 2 K, steeply decreased on warming, and then disappeared at 5.6 K. The large discrepancy of M_{mol} value between the FCM and the ZFCM measurements indicated the long-range magnetic ordering of the magnetic spin. From the divergent point of the FCM and the ZFCM measurements, the critical temperature, T_c, was determined to be 5.6 K. Similar thermal profiles of the M_{mol} value in ZFCM, FCM, and RM cycles were observed in **5**, **7**, and **8**, whose T_c values were 4.0, 4.0, and 6.2 K, respectively. The large discrepancy of M_{mol} value in FCM and the ZFCM and the observation of the M_{mol} value in RM suggested a transition to canted 2D or 3D antiferromagnets below T_c. Such magnetic behaviors are often observed in anisotropic metal complexes in low[5c,f,17] and high dimensional[18] complexes. In contrast, in complexes, **2**, **3**, **4**, and **6**, the M_{mol} values in ZFCM and FCM measurements showed the same temperature dependence and no divergent points were observed above 1.9 K. Complexes **2** and **3** showed broad maxima (2.2 cm^3 Oe mol^{-1} at 10.5 K and 6.9 cm^3 Oe mol^{-1} at 4.2 K, respectively) and **4** and **6** showed a continuous increase in χ_{mol} until 1.9 K. **6** might have had a maximum at the temperature just below 1.9 K. These results suggested that the complexes **2**, **3**, **4**, and **6** are ferromagnetic chains above 1.9 K and that the resulting chains of **2**, **3**, and **6** are affected by interchain antiferromagnetic interaction below 10 and 4 K, and near 1.9 K, respectively. To better understand the magnetic properties of **4**, dc magnetic susceptibility measurement in the temperature range of 0.46−1.9 K at the constant field of 50 Oe was carried out. In the χ_{mol} vs T plot, the χ_{mol} values gradually increased on cooling, and separated into two near the maximum (30 $cm^3\ mol^{-1}$) at 1.0 K. No steep increase of the χ_{mol} values because of the magnetic transition was observed below 1.9 K. The observed divergence point might be a blocking temperature, T_B, because of the slow magnetic behavior, and the T_B value was determined to be 1.0 K. The data for χ_{mol} in the range of 1.9−5 K and 0.46−1.9 K were combined and are shown in Supporting Information, Figure S8.

These ZFCM, FCM, and RM measurements indicated that complexes **1**, **5**, **7**, and **8** are canted 2D antiferromagnets below T_c values of 5.6, 4.0, 4.0, and 6.2 K, respectively, **2**, **3**, and **6** are ferromagnetic chains having interchain antiferromagnetic interaction, and **4** is a nearly isolated ferromagnetic chain.

From the results of X-ray structure, the inversion centers existed between the chains in crystal structures for all complexes. However, the complexes **1**, **5**, **7**, and **8** showed behaviors of canted antiferromagnets. In complex **1**, antiferromagnetic interaction took place between the anisotropic chains without inversion center. Therefore, the spin canting was observed. In **5**, **7**, and **8**, on the other hand, the inversion centers disappeared by the formation of the *P*- and *M*-helical chains, and spin cantings were produced by antiferromagnetic interaction between the *P*- and *M*-helical chains. Schematic drawings for the relation between the interchain magnetic interaction and the crystal packings are shown in Supporting Information, Figure S9.

(iii). Plots of $M_{mol}/N\mu_B$ vs H. The dc field dependencies of the molar magnetization, M_{mol}, at 1.9 K for the complexes **1**−**8**

dx.doi.org/10.1021/ic202397m | Inorg. Chem. 2012, 51, 4982−4993

were measured in the field range of 0−50 kOe. The plots of $M_{mol}/N\mu_B$ vs H together with dM/dH vs H are shown in Figure 9.

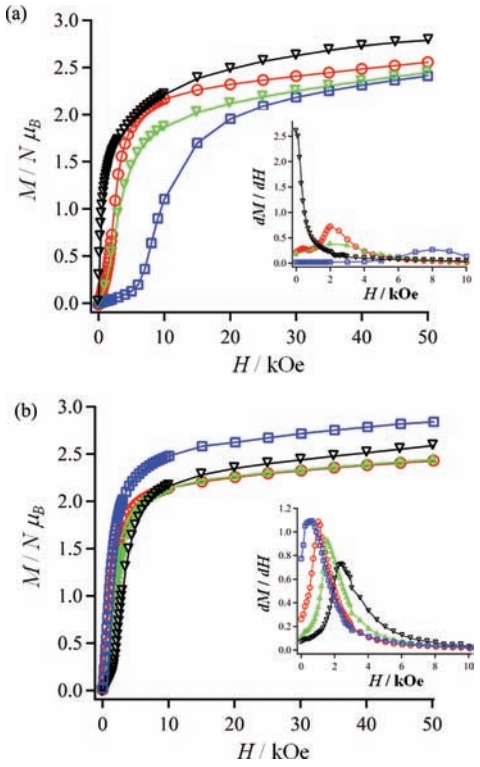

Figure 9. Plots of $M_{mol}/N\mu_B$ vs H at 1.9 K for (a) **1** (red), **2** (blue), **3** (green), and **4** (black) and (b) **5** (red), **6** (blue), **7** (green), and **8** (black). Insets show dM/dH vs H plots. Solid lines are guides for the eyes.

In the $M_{mol}/N\mu_B$ vs H plots at 1.9 K for the chains except **4**, the $M_{mol}/N\mu_B$ values increased gradually in a sigmoid shape in low field (<10 kOe) and linearly increased until 50 kOe. The values did not reach the saturation magnetization, M_s, even at 50 kOe. The values of $M_{mol}/N\mu_B$ at 50 kOe were 2.56, 2.41, 2.45, and 2.79 for **1**, **2**, **3**, and **4**, respectively, in trans complexes, and 2.43, 2.84, 2.44, and 2.56 for **5**, **6**, **7**, and **8**, respectively, in cis complexes. It was noted that the values at 50 kOe for **4** and **6** were large compared with the others. The increase in sigmoid shape typical to a metamagnet suggested the presence of antiferromagntic interactions. In the dM/dH vs H plots for **1**, two maxima were observed at 1.0 and 2.2 kOe. On warming, the peak at 2.2 kOe indicating the critical fields, H_{cr}, shifted to the lower field, while the alteration of the peak at 1.0 kOe was not clear (Supporting Information, Figure S10). The data in the dM/dH vs H plots at various temperatures using the peak at 2.2 kOe, the peak-top temperatures in the χ_{mol} vs T plots at the constant field of 0.5, 1.0, 1.5 kOe, and the frequency-independent χ_{mol}'' peaks in the following ac measurements were combined and the (T, H) phase diagram for **1** was obtained (Figure 10). In the phase diagram, the H_{cr} value of 2.2 kOe at 1.9 K gradually decreased on warming, abruptly decreased above 5 K, and then disappeared at 5.6 K. The observed thermal profile of H_{cr} showed a typical AF-P transition line in metamagnetic complexes. From the dM/dH vs H plots for the other complexes, the values of H_{cr} at 1.9 K were determined to be 8.0 and 2.4 kOe for **2** and **3**,

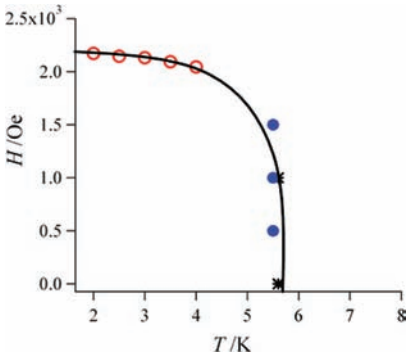

Figure 10. (T, H) phase diagram for **1**; the data from the dM/dH vs T plot at various temperatures (open red circle), from the χ_{mol} vs T plots at constant dc fields of 0.5, 1.0, and 1.5 kOe (filled blue circle), and from ac susceptibility experiments (*). The solid line is a guide for the eyes.

respectively, in trans complexes and 1.0, 0.6, 1.5, and 2.4 kOe for **5**, **6**, **7**, and **8**, respectively, in cis complexes. The H_{cr} for **4** was not observed. The (T, H) phase diagrams of **2**, **3**, **5**, **7**, and **8** are shown in Supporting Information, Figure S10′.

Since the observed magnetic behaviors were metamagnet-like because of the interchain antiferromagnetic interaction,[19] the values of the antiferromagnetic coupling parameter, $|zJ'|$, can be estimated by the equation; $g_{\|}\mu_B SH_{cr} = 2|zJ'|S^2$, where $g_{\|}$ and z are the parallel g value and the number of the coupled chains, respectively.[20] The $g_{\|}$ value was estimated from $C \approx C_{eff} = N\mu_B{}^2 g_{\|} S^2/3k$. The obtained $|zJ'|$ values for **1**−**3** and **5**−**8** are listed in the Table 2 together with the Tc, Hcr, and $g_{\|}$ values.

Table 2. Values of T_c, H_{cr}, and $|zJ'|/k_B$ for 1−4 and 5−8

	1	2	3	4	5	6	7	8
T_c (K)	5.5				4.0		4.2	6.2
H_c (kOe)	0.4, 2.2	8.0	2.4		1.0	0.6	1.5	2.4
$\|zJ'\|/k_B$	0.35	1.26	0.41		0.16	0.10	0.25	0.41
$g_{\|}$[a]	4.8	4.7	5.1	5.1	4.9	5.0	5.0	5.1

[a] $g_{\|}$ value was estimated from $C \approx C_{eff} = N\mu_B{}^2 g_{\|} S^2/3k$.

Weak interchain antiferromagnetic interactions observed in these dc magnetic measurements might be caused by the proximity of the neighboring chains. In the crystal structures of these complexes, short NO-C_β contacts (3.25 and 3.26 Å) were observed in **1** and **2** (Supporting Information, Figure S4), and the short distances were found within 3.6 Å between the NO and the halogen in **2**−**8**.

Magnetic Properties of the Aligned Sample of 6. To determine the magnetic axis in the chain, the angular dependence of the magnetizations was investigated at 1.9 K. Ten pieces of small-sized single crystals (ca. 0.1 mg) of **6** were used and aligned on a sample holder. Since the symmetry of the crystal structure for **6** is monoclinic with $P2_1/c$, the b axis was one of magnetic axes and the other two would exist in the plane perpendicular to the b axis.[3d,21] The magnetizations were measured at the constant field of 1 kOe at 1.9 K in the ac and ab planes with the crystal rotating along the b and c axis, respectively (Figure 11). As the β angle in a unit cell is 94°, the a^* axis perpendicular to the bc plane is close to the a axis.

As shown in Figure 11, the extremes were found to be roughly along the a^* (θ = 90 and 270, maxima) and c (θ = 0 and 180, minima) direction in the rotation around the b axis

dx.doi.org/10.1021/ic202397m | Inorg. Chem. 2012, 51, 4982−4993

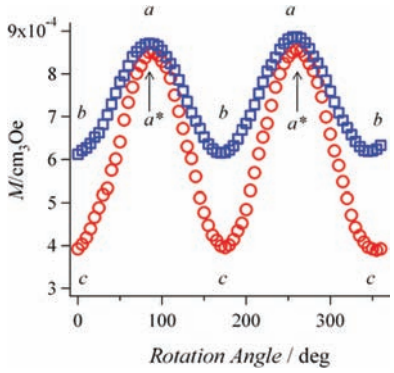

Figure 11. Angular dependence of magnetization of the aligned crystal sample for **6** with $_{Hdc}$ = 1 kOe at 1.9 K in *ac* (red) and *ab* planes (blue).

and along the *a* (θ = 90 and 270, maxima) and *b* (θ = 0 and 180, minima) directions in the rotation around the *c* axis. From these results, the magnetic axes were determined to be the crystallographic axes, *a**, *b*, and *c*.

The temperature and field dependences of magnetization for the aligned sample of **6** were investigated by applying the dc field along the *a**, *b*, and *c* axes, *a**||*H*, *b*||*H*, and *c*||*H*, respectively. The plots of *MT* vs *T* and *M*/*Ms* vs *H* are shown in Supporting Information, Figure S11. In the *MT* vs *T* plot at constant field of 1.0 kOe, the thermal profile of the *MT* values was similar to that for the powdered sample. However, the magnitude of *MT* values strongly depended on the direction of applied field and decreased in order of applied dc field as *a**||*H* > *b*||*H* > *c*||*H*. In the *M*/*Ms* vs *H* plot at 1.9 K, the magnetization curves also strongly depended on the direction of field application. The magnitude ratio of the *M* values at 50 kOe were 1:0.85:0.65 for *a**||*H*, *b*||*H*, and *c*||*H*. The observed thermal and field profiles of *M* values depending on the direction of dc field application suggested that the magnetic easy axis was the direction of the *a** axis close to the *a* axis among the *a*, *b*, and *c* axes of the crystal, and the spin system for **6** was not fulfilled by the Ising 1D model. As the axis of the helical chain of **6** was the *b* axis, the magnetic easy axis was coincident neither with the direction of the chain in the crystal nor with local anisotropic axis, the *z* axis of O−Co−O, for cobalt ion. The angles between the *z* axis of O−Co−O and the *a*, *b*, and *c* axes were 39, 69, and 64°, respectively, and the angle of *z*-*a* was the smallest.

(B-2). Dynamic Magnetic Properties of ***1*****−****8*****.*** The ac magnetic susceptibilities (χ'_{mol} and χ''_{mol} for the in-phase and the out-of-phase signals, respectively) with a 3.9 or 4.9 Oe ac field at a frequency range of 1−997 Hz in the absence and the presence of dc field were measured in the temperature range of 1.9−8.0 K. In the ac magnetic susceptibility measurements for powder samples of all complexes, χ'_{mol} and χ''_{mol} signals with frequency dependence were observed. The H_{cr} values obtained from d*M*/d*H* vs *H* plots were used as applied dc fields.

Complex ***1*****.** The ac magnetic susceptibility for **1** was measured with H_{dc} = 0.0, 1.0, and 2.2 kOe and the χ'_{mol} vs *T* and χ''_{mol} vs *T* plots are shown in Figure 12.

In χ''_{mol} vs *T* plots with H_{dc} = 0, two maxima of the χ''_{mol} signals were observed at 5.6 and below about 4 K. A relatively sharp maximum at 5.6 K did not depend on the frequency, while broad maxima depended on the frequency and maxima shifted to the low temperature with decreasing the frequency. The former and the latter were due to the phase transition to

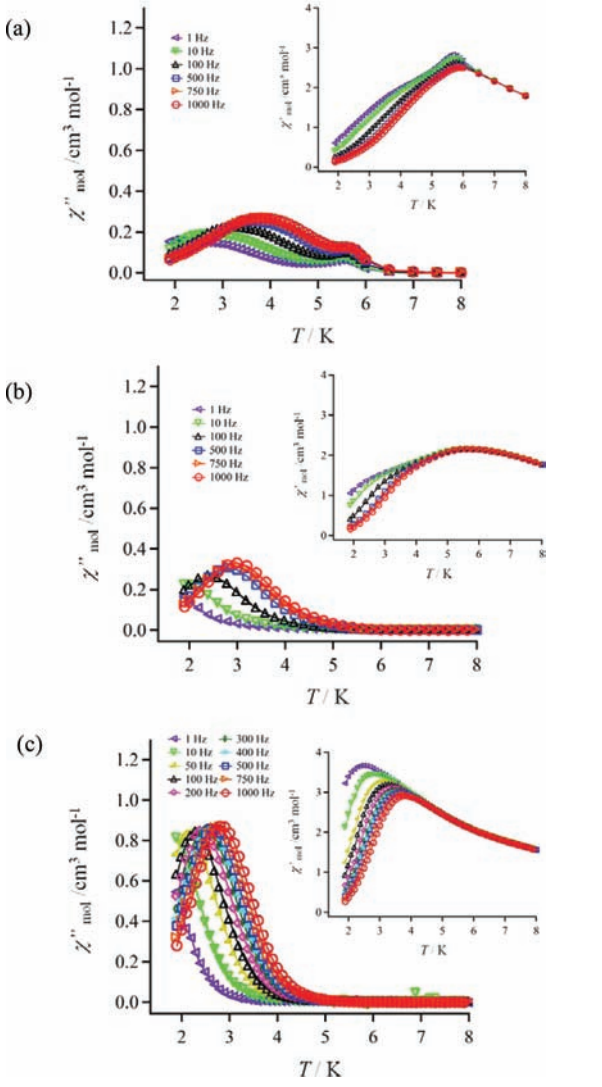

Figure 12. χ''_{mol} vs *T* plots at given frequencies for **1** with H_{dc} = 0 (a), 1.0 (b), and 2.2 kOe (c). Insets show χ'_{mol} vs *T* plots. Solid lines are guides for the eyes.

antiferromagnet[17] and the magnetic slow relaxation, respectively. The peak-top temperature of 5.6 K was in good agreement with the T_c values obtained from ZFCM, FCM, and RM measurements. When the dc fields were applied, the χ'_{mol} vs *T* and χ''_{mol} vs *T* plots drastically changed. The peaks of the χ'_{mol} and χ''_{mol} signals at 5.6 K disappeared, and the peak-top temperature of both signals shifted to the low temperature by an applied dc field of 1.0 kOe, and then the intensity increased by an applied dc field of 2.2 kOe.

Complexes, ***2*****−****4*****.*** In χ''_{mol} vs *T* plots for **2** and **3** with H_{dc} = 0, the frequency dependence of χ''_{mol} signals with extremely weak intensity were observed. However, the maxima of the signals could not be observed above 1.9 K, which is the lowest temperature possible with our apparatus. In contrast, χ''_{mol} vs *T* plots changed in the presence of H_{dc}. The χ''_{mol} signals for **2** and **3** showing the maxima above 1.9 K appeared with applied dc field of 8.0 and 1.5 kOe, respectively. However, the intensities of the maxima of the χ''_{mol} signals were still weak and decreased with decreasing frequency. The χ''_{mol} vs *T* plots in the presence of H_{dc} might suggest that the contribution of interchain antiferromagnetic interaction still remained. In **4**, on the other

dx.doi.org/10.1021/ic202397m | *Inorg. Chem.* 2012, 51, 4982−4993

hand, χ''_{mol} signals depending on frequency below 2.6 K were observed, but the peak tops were not observed even at 1000 Hz above 1.9 K in the absence of a dc field. When a dc field of 0.1 kOe was applied, no significant changes of the maximum of the χ''_{mol} signals were observed. Complex **4** was considered to have peak-top temperatures below 1.9 K. The χ''_{mol} vs T plots with H_{dc} = 0 and 8.0 kOe for **2** and the χ'_{mol} vs T and χ''_{mol} vs T plots with H_{dc} = 0 for **4** are shown in Figure 13. The corresponding

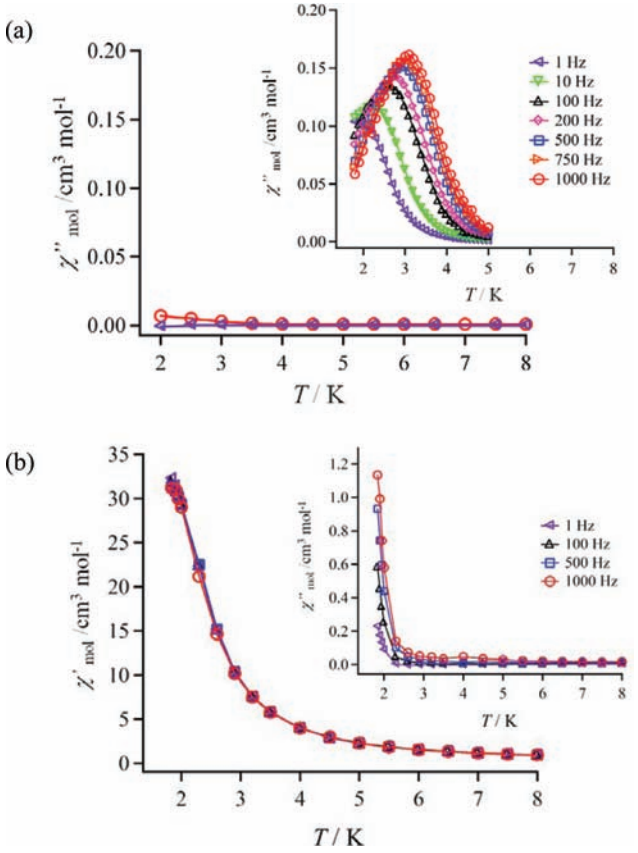

Figure 13. (a) χ''_{mol} vs T plot for **2** at given frequencies with H_{dc} = 0 kOe and 8.0 kOe (inset) and (b) χ'_{mol} vs T and χ''_{mol} vs T (inset) plot for **4** at given frequencies with H_{dc} = 0 kOe. Solid lines are guides for the eyes.

χ'_{mol} vs T plot for **2**, the χ'_{mol} vs T and χ''_{mol} vs T plots for **3** with H_{dc} = 0, 1.5, and 2.4 kOe, and the χ'_{mol} vs T and χ''_{mol} vs T plots for **4** with H_{dc} = 0.1 kOe are shown in the Supporting Information, Figure S12.

*Complexes, **5**–**8**.* In the χ''_{mol} vs T plots with H_{dc} = 0 for **5**, **7**, and **8**, the thermal profiles of the χ''_{mol} signals were similar to that for **1**. The intensities of the χ''_{mol} signals at the peak-top temperature decreased with decreasing frequency. Additional temperature-independent peaks were also observed at 3.6, 4.6, and 5.5 K for **5**, **7**, and **8**, respectively, which were also in good agreement with the T_c values observed from ZFCM, FCM, and RM measurements. The χ'_{mol} vs T and χ''_{mol} vs T plots for **5**, **7**, and **8** for applied-dc field of 1.0, 1.5, and 2.4 kOe, respectively, changed to the typical plots for SMM, SCM,[20,22] and spin glass,[23] and the additional maximum peaks of the χ'_{mol} and χ''_{mol} signals disappeared. Complex **6** showed no temperature-independent peak and no noticeable difference in the χ''_{mol} vs T plot between the absence and presence of a dc field of 0.6 kOe. Somehow an increase of the maximum χ''_{mol} signal in the low temperature region was observed. The χ''_{mol} vs T plots for **5** and **6** in the absence and the presence of dc field are demonstrated in Figure 14. The corresponding χ'_{mol} vs T plots

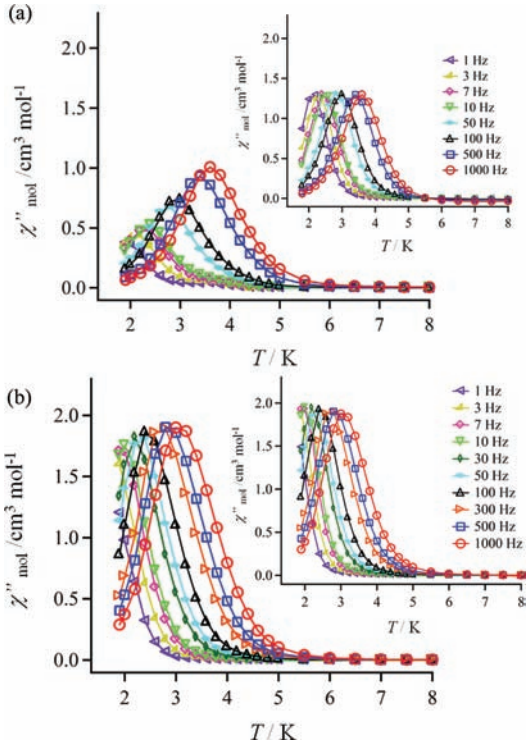

Figure 14. χ''_{mol} vs T plots at given frequencies for **5** (a) and **6** (b) with H_{dc} = 0 kOe. Insets show the χ''_{mol} vs T plots in the presence of H_{dc} = 1.0 (a) and 0.6 kOe (b). Solid lines are guides for the eyes.

for **5** and **6** and the χ'_{mol} vs T and χ''_{mol} vs T plots for **7** and **8** are shown in the Supporting Information, Figure S13.

The decay data obtained from the peak-top temperature of χ''_{mol} signals at each frequency linearly decreased according to the Arrehnius law; $\tau = 1/2\pi\nu = \tau_0 \exp(\Delta_{eff}/k_BT)$ (Supporting Information, Figure S14). The values of the thermal activation barrier, Δ_{eff}/k_B, and the preexponential factor, τ_0, in the absence and the presence of dc field are listed in Table 3.

The thermal profiles in the χ'_{mol} vs T and χ''_{mol} vs T plots for all complexes in the presence of a dc field were close to those typical to SMM, SCM,[20,22] and spin glass[23] The τ_0 values were more than 10^{-10} s and were physically reasonable, which excluded the possibility of a spin glass. The obtained Δ_{eff}/k_B values for **1**–**8** except **4** were in the range of 25–39 K in the presence of 0.6–8.0 kOe, and the values for cis chains were slightly larger than those for trans chains. It was noted that the obtained Δ_{eff}/k_B values were comparable with U_{eff}/k_B = 29 K for the discrete SMM complex, $[Co(hfpip)_2(\mathbf{4NOpy})_2]$.[9] In an Ising 1D model[3b] of the chain for SCM, the activation barrier, Δ_{eff}/k_B, in a finite length region is expressed as the equation, $\Delta_{eff}/k_B = \Delta_\xi/k_B + \Delta_a/k_B$; Δ_ξ/k_B and Δ_a/k_B are the correlation length energy and an anisotropic energy, respectively. The Δ_ξ/k_B value can be estimated from the ln $\chi'_{mol}T$ vs T^{-1} plot. The linear fitting in the ln $\chi'T$ vs T^{-1} plot for **6**, which had the smallest contribution of the interchain antiferromagnetic interaction in these chains except **4**, gave 17 K for Δ_ξ/k_B corresponding to $4JS^2$ (Supporting Information, Figure S15). The value of 17 K was significantly smaller than that (46 K) calculated by using J/k_B = 11.5 K and S = 2/2, indicating that

dx.doi.org/10.1021/ic202397m | Inorg. Chem. 2012, 51, 4982–4993

Table 3. Values of Δ_{eff}/k_B and τ_0 in the Absence and Presence of a dc Field[a]

	H_{dc} (kOe)	Δ_{eff}/k_B (K)	τ_0 (sec)
1	0.0	56.4	6.8×10^{-11}
	1.0	28.8	1.1×10^{-8}
	2.2	27.4	1.1×10^{-8}
2	0.0	n.e.	n.e.
	8.0	39.0	4.0×10^{-10}
3	0.0	n. e.	n. e.
	1.5	24.5	2.7×10^{-10}
	2.4	n. e.	n. e.
4	0.0	n. e.	n. e.
	0.1	n. e.	n. e.
5	0.0	24.5	5.4×10^{-7}
	1.0	36.3	7.4×10^{-9}
6	0.0	29.6	1.2×10^{-8}
	0.6	26.9	2.8×10^{-8}
7	0.0	23.9	1.3×10^{-7}
	1.5	39.2	1.2×10^{-9}
8	0.0	18.4	2.9×10^{-7}
	2.4	31.2	5.0×10^{-9}

[a] n. e.: not estimated.

these spin systems were not fulfilling the Ising 1D model. When the Δ_{eff}/k_B and Δ_{ξ}/k_B values for **6** were 27 and 17 K, respectively, the relation between the energy gaps afforded 10 K for Δ_a/k_B, which was very different from U_{eff}/k_B = 29 K for $[Co(hfpip)_2(\mathbf{4NOpy})_2]$.[9] This discrepancy might suggest that an anisotropic energy largely varied by forming the chain structure. The dynamic magnetic properties in these heterospin chains might be strongly affected by the difference in the directions between the chain axis and the local spin anisotropy of the cobalt ions (Figure 15).

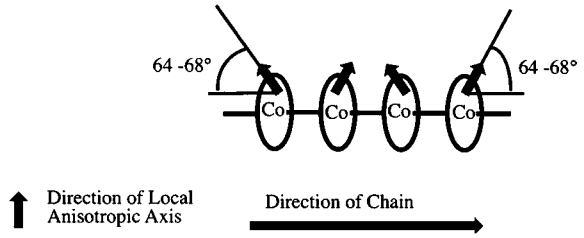

Figure 15. Schematic drawing of the directions of the local anisotropic axis and the chain axis in heterospin chains, **1**–**8**.

CONCLUSION

For the construction of anisotropic 1D chains in heterospin systems, a new bridging ligand having an aminoxyl, **NOpy$_2$**, was successfully prepared. The cobalt(II) complexes, $[Co(hfpip\text{-}X)_2(\mathbf{NOpy_2})]_n$, X = H (**1**), F (**2**), F_3 (**3**), F_5 (**4**), Cl (**5**), Cl_3 (**6**), Br (**7**), and I (**8**), were obtained from the 1:1 solution mixtures of **NOpy$_2$** and $Co(hfpip\text{-}X)_2$. The cobalt-complex units in all complexes were compressed octahedra, in which the bond lengths (r_{Co-O}) were shorter by 0.2 Å than the others. The pyridine moieties in **NOpy$_2$** units coordinated to the cobalt ions in trans configuration to form linear chains for **1**–**4** and in cis configuration to form helical chains for **5**–**8**. In all complexes, the aminoxyl in **NOpy$_2$** interacted ferromagnetically with the cobalt ions through both sides of the pyridine rings to produce ferromagnetic chains. Furthermore, all complexes except for **4** had interchain antiferromagnetic interactions caused by the proximity of the chains. The static magnetic properties of **1**, **5**, **7**, and **8**, were canted 2D antiferromagnets with T_c = 5.6, 4.0, 4.0, and 6.2 K, respectively, while **2**, **3**, and **6** were ferromagnetic chains showing metamagnet-like behaviors and **4** was a nearly isolated ferromagnetic chain. In dynamic ac magnetic susceptibility measurements for all complexes, χ'_{mol} and χ''_{mol} signals with frequency dependence indicative of slow magnetic relaxation were observed. However, the observed thermal profiles of the χ''_{mol} signals strongly depended on the dc field. The activation barriers of Δ_{eff}/k_B for the reorientation of the spin were 25–39 K for all complexes except **4** in the presence of a dc field of 0.6–8.0 kOe. The Δ_{eff}/k_B value for **4** could not be determined, because the peak-top temperatures of the χ''_{mol} signals were below 1.9 K. The obtained Δ_{eff}/k_B values were comparable to that of 29 K for $[Co(hfpip)_2(\mathbf{4NOpy})_2]$[9] obtained in frozen solution. The small activation barriers for these heterospin chains were considered to be due to the discrepancy of direction between the chain axis and the local anisotropic axis. In these chains, the local anisotropic axes for the cobalt ions were directed at a large angle (z-b = 64–68°) to the chain axis (the b axis). For the construction of a heterospin 1D chain with large activation barrier, therefore, the anisotropic axis for the cobalt complex units was required to be aligned to the chain direction. For this purpose, the design and preparation of a new magnetic coupler are in progress.

ASSOCIATED CONTENT

Supporting Information

X-ray crystallographic files in the CIF format for **NOpy$_2$** and complexes **1**–**8**, experimental details (S1), X-ray crystallographic information (S2–S6), and the results of various magnetic measurements (S7–S18) for **1**–**8**. This material is available free of charge via the Internet at http://pubs.acs.org.

AUTHOR INFORMATION

Corresponding Author

*E-mail: koga@fc.phar.kyushu-u.ac.jp.

Notes

The authors declare no competing financial interest.

ACKNOWLEDGMENTS

The authors acknowledge Dr. H. Shirakawa of National Institute of Advanced Industrial Science and Technology and Mr. T. Ota of IQUANTUM Co. LTD. for the SQUID measurements below 2 K and Dr. K. Yoza of Bruker AXS Co. LTD. for useful discussion on X-ray crystallography for complexes **2** and **4**. This work was supported by the "Nanotechnology Support Project" of the Ministry of Education, Culture, Sports, Science and Technology (MEXT), Japan.

REFERENCES

(1) Kahn, O. *Molecular Magnetism*; Wiley-VCH Publishers: Weinheim, Germany, 1993.

(2) (a) Christou, G.; Gatteschi, D.; Hendrickson, D. N.; Sessoli, R. *MRS Bull.* **2000**, *25*, 66–71. (b) Yoo, J.; Brechin, E. K.; Yamaguchi, A.; Nakano, M.; Huffman, J. C.; Maniero, A. L.; Brunel, L.-C.; Awaga, K.; Ishimoto, H.; Christou, G.; Hendrickson, D. N. *Inorg. Chem.* **2000**, *39*, 3615–3623. (c) Aubin, S. M. J.; Dilley, N. R.; Pardi, L.; Krzystek, J.; Wemple, M. W.; Brunel, L.-C.; Maple, M.; Christou, G.; Hendrickson, D. N. *J. Am. Chem. Soc.* **1998**, *120*, 4991–5004. (d) Brechin, E. K.;

Boskovic, C.; Wernsdorfer, W.; Yoo, J.; Yamaguchi, A.; Sanudo, E. C.; Concolino, T. R.; Rheingold, A. L.; Ishimoto, H.; Hendrickson, D. N.; Christou, G. *J. Am. Chem. Soc.* **2002**, *124*, 9710−9711. (e) Tasiopoulos, A. J.; Vinslava, A.; Wernsdorfer, W.; Abboud, K. A.; Christou, G. *Angew. Chem., Int. Ed.* **2004**, *43*, 2117−2121. (f) Murugesu, M.; Habrych, M.; Wernsdorfer, W.; Abboud, K. A.; Christou, G. *J. Am. Chem. Soc.* **2004**, *126*, 4766−4767. (g) Chakov, N. E.; Lee, S.-C.; Harter, A. G.; Kuhns, P. L.; Reyes, A. P.; Hill, S. O.; Dalal, N. S.; Wernsdorfer, W.; Abboud, K. A.; Christou, G. *J. Am. Chem. Soc.* **2006**, *128*, 6975−6989. (h) Milios, C. J.; Vinslava, A.; Wood, P. A.; Parsons, S.; Wernsdorfer, W.; Christou, G.; Perlepes, S. P.; Brechin, E. K. *J. Am. Chem. Soc.* **2007**, *129*, 8−9. (i) Miyasaka, H.; Clérac, R.; Wernsdorfer, W.; Lecren, L.; Bonhomme, C.; Sugiura, K.; Yamashita, M. *Angew. Chem., Int. Ed.* **2004**, *43*, 2801−2805. (j) Ishikawa, N.; Sugita, M.; Wernsdorfer, W. *J. Am. Chem. Soc.* **2005**, *127*, 3650−3651.

(3) (a) Caneschi, A.; Gatteschi, D.; Lalioti, N.; Sangregorio, C.; Sessoli, R.; Venturi, G.; Vindigni, A.; Rettori, A.; Pini, M. G.; Novak, M. A. *Angew. Chem., Int. Ed.* **2001**, *40*, 1760−1763. (b) Clérac, R.; Miyasaka, H.; Yamashita, M.; Coulon, C. *J. Am. Chem. Soc.* **2002**, *124*, 12837−12844. (c) Miyasaka, H.; Julve, M.; Yamashita, M.; Clérac, R. *Inorg. Chem.* **2009**, *48*, 3420−3437. (d) Bermot, K.; Luzon, J.; Sessoli, R.; Vindigni, A.; Thion, J.; Richeter, S.; Leclercq, D.; Larionova, J.; van der Lee, A. *J. Am. Chem. Soc.* **2008**, *130*, 1619−1627. (e) Lescouëzec, R.; Vaissermann, J.; Ruiz-Pérez, C.; Lloret, F.; Carrasco, R.; Julve, M.; Verdaguer, M.; Dromzee, Y.; Gatteschi, D.; Wernsdorfer, W. *Angew. Chem., Int. Ed.* **2003**, *42*, 1483−1486. (f) Palii, A. V.; Ostrovsky, S. M.; Klokishner, S. I.; Reu, O. S.; Sun, Z.-M.; Prosvirin, A. V.; Zhao, H.-H.; Mao, J.-G.; Dunbar, K. R. *J. Phys. Chem. A.* **2006**, *110*, 14003−14012. (g) Wernsdorfer, W.; Clérac, R.; Coulon, C.; Lecren, L.; Miyasaka, H. *Phys. Rev. Lett.* **2005**, *95*, 237203. (h) Toma, L. M.; Lescouëzec, R.; Pasán, J.; Ruiz-Pérez, C.; Vaissermann, J.; Cano, J.; Carrasco, R.; Wernsdorfer, W.; Lloret, F.; Julve, M. *J. Am. Chem. Soc.* **2006**, *128*, 4842−4853.

(4) (a) Koga, N.; Karasawa, S. *Bull. Chem. Soc. Jpn.* **2005**, *78*, 1384−1400. (b) Karasawa, S.; Kumada, H.; Koga, N.; Iwamura, H. *J. Am. Chem. Soc.* **2001**, *123*, 9685−9686. (c) Karasawa, S.; Koga, N. *Polyhedron* **2003**, *22*, 1877−1882. (d) Morikawa, H.; Karasawa, S.; Koga, N. *Appl. Magn. Reson.* **2003**, *23*, 507−515. (e) Karasawa, S.; Koga, N. *Polyhedron* **2001**, *20*, 1387−1389. (f) Morikawa, H.; Imamura, F.; Tsurukami, Y.; Itoh, T.; Kumada, H.; Karasawa, S.; Koga, N.; Iwamura, H. *J. Mater. Chem.* **2001**, *11*, 493−502.

(5) (a) Karasawa, S.; Zhou, G.; Morikawa, H.; Koga, N. *J. Am. Chem. Soc.* **2003**, *125*, 13676−13677. (b) Karasawa, S.; Koga, N. *Inorg. Chem.* **2011**, *50*, 5186−5195. (c) Kanegawa, S.; Karasawa, S.; Nakano, M.; Koga, N. *Bull. Chem. Soc. Jpn.* **2006**, *79*, 1372−1382. (d) Kanegawa, S.; Karasawa, S.; Nakano, M.; Koga, N. *Chem. Commun.* **2004**, 1750−1751. (e) Yoshihara, D.; Karasawa, S.; Koga, N. *J. Am. Chem. Soc.* **2008**, *130*, 10460−10461. (f) Kanegawa, S.; Karasawa, S.; Maeyama, M.; Nakano, M.; Koga, N. *J. Am. Chem. Soc.* **2008**, *130*, 3079−3094. (g) Yoshihara, D.; Karasawa, S.; Koga, N. *Polyhedron* **2011**, *30*, 3211−3217. (h) Tobinaga, H.; Suehiro, M.; Ito, T.; Zhou, G.; Karasawa, S.; Koga, N. *Polyhedron* **2007**, *26*, 1905−1911.

(6) Sano, Y.; Tanaka, M.; Koga, N.; Matsuda, K.; Iwamura, H.; Rabu, P.; Drillon, M. *J. Am. Chem. Soc.* **1997**, *119*, 8246−8252.

(7) Karasawa, S.; Sano, Y.; Akita, T.; Koga, N.; Itoh, T.; Iwamura, H.; Rabu, P.; Drillon, M. *J. Am. Chem. Soc.* **1998**, *120*, 10080−10087.

(8) Karasawa, S.; Koga, N. *Inorg. Chem.* **2011**, *50*, 2055−2057.

(9) Karasawa, S.; Yoshihara, D.; Watanabe, N.; Nakano, M.; Koga, N. *Dalton Trans.* **2008**, 1418−1420.

(10) Kitano, M.; Ishimaru, Y.; Inoue, K.; Koga, N.; Iwamura, H. *Inorg. Chem.* **1994**, *33*, 6012−6019.

(11) Liu, Y.-H.; Cheng, Y.-C.; Tung, Y.-L.; Chi, Y.; Chen, Y.-L.; Liu, C.-S.; Peng, S.-M.; Lee, G.-H. *J. Mater. Chem* **2003**, *13*, 135−142.

(12) Bondi, A. *J. Phy. Chem.* **1964**, *68*, 441−451.

(13) Duling, D. R. *J. Magn. Reson., B* **1994**, *104*, 105−110.

(14) (a) Estes, W. E.; Gavel, D. P.; Hatfield, W. E.; Hodgson, D. J. *Inorg. Chem.* **1978**, *17*, 1415−1421. (b) Hayashi, H.; Karasawa, S.; Koga, N. *J. Org. Chem.* **2008**, *73*, 8683−8693.

(15) (a) van Koningsbruggen, P. J.; Kahn, O.; Nakatani, K.; Yu, P.; Renard, J. P.; Drillon, M.; Legoll, P. *Inorg. Chem.* **1990**, *29*, 3325−3331. (b) Pardo, E.; Ruiz-García, R.; Lloret, F.; Faus, J.; Julve, M.; Journaux, Y.; Delgado, F.; Ruiz-Pérez, C. *Adv. Mater.* **2004**, *16*, 1597−1600. (c) Ferrando-Soria, J.; Pardo, E.; Ruiz-García, R.; Cano, J.; Lloret, F.; Julve, M.; Journaux, Y.; Pasán, J.; Ruiz-Pérez, C. *Chem.—Eur. J.* **2011**, *17*, 2176−2188. (d) Pardo, E.; Ruiz-García, R.; Lloret, F.; Faus, J.; Julve, M.; Journaux, Y.; Novak, M. A.; Delgado, F. S.; Ruiz-Pérez, C. *Chem.—Eur. J.* **2007**, *13*, 2054−2066.

(16) (a) Figgis, B. N.; Hitchman, M. A. *Ligand Field Theory and Its Application*; Wiley-VCH Publishers: New York, 2000. (b) Lloret, F.; Julve, M.; Cano, J.; Ruiz-García, R.; Pardo, E. *Inorg. Chim. Acta* **2008**, *361*, 3432−3445.

(17) (a) Manson, J. L.; Huang, Q.-z.; Lynn, J. W.; Koo, H.-J.; Whangbo, M.-H.; Bateman, R.; Otsuka, T.; Wada, N.; Argyriou, D. N.; Miller, J. S. *J. Am. Chem. Soc.* **2001**, *123*, 162−172. (b) Miller, J. S.; Manson, J. L. *Acc. Chem. Res.* **2001**, *34*, 563−570. (c) Manson, J. L.; Kmety, C. R.; Epstein, A. J.; Miller, J. S. *Inorg. Chem.* **1999**, *38*, 2552−2553. (d) Takagami, N.; Ishida, T.; Nogami, T. *Bull. Chem. Soc. Jpn.* **2004**, *77*, 1125−1134. (e) King, P.; Clérac, R.; Anson, C. E.; Coulon, C.; Powell, A. K. *Inorg. Chem.* **2003**, *42*, 3492−3500.

(18) (a) Miyasaka, H.; Takayama, K.; Saitoh, A.; Furukawa, S.; Yamashita, M.; Clérac, R. *Chem.—Eur. J.* **2010**, *16*, 3656−3662. (b) Liu, C.-M.; Zhang, D.-Q.; Zhu, D.-B. *Inorg. Chem.* **2009**, *48*, 4980−4987. (c) Miyasaka, H.; Nakata, K.; Lecren, L.; Coulon, C.; Nakazawa, Y.; Fujisaki, T.; Sugiura, K.; Yamashita, M.; Clérac, R. *J. Am. Chem. Soc.* **2006**, *128*, 3770−3783.

(19) (a) Toma, L. M.; Lescouëzec, R.; Lloret, F.; Julve, M.; Vaissermann, J.; Verdaguer, M. *Chem. Commun.* **2003**, 1850−1851. (b) Liu, T.; Zhang, Y.-Z.; Kanegawa, S.; Sato, O. *J. Am. Chem. Soc.* **2010**, *132*, 8250−8251.

(20) Wang, Y.-Q.; Zhang, X.-M.; Li, X.-B.; Wang, B.-W.; Gao, E.-Q. *Inorg. Chem.* **2011**, *50*, 6314−6322.

(21) Wang, X.-Y.; Wang, Z.-M.; Gao, S. *Inorg. Chem.* **2008**, *47*, 5720−5726.

(22) (a) Mahata, P.; Natarajan, S.; Panissod, P.; Drillon, M. *J. Am. Chem. Soc.* **2009**, *131*, 10140−10150. (b) Coulon, C.; Clérac, R.; Wernsdorfer, W.; Colin, T.; Miyasaka, H. *Phys. Rev. Lett.* **2009**, *102*, 167204.

(23) Zhu, Z.; Karasawa, S.; Koga, N. *Inorg. Chem.* **2005**, *44*, 6004−6011.